



## Full Text View

[Volume 31, Issue 12 \(December 2001\)](#)

### Journal of Physical Oceanography

Article: pp. 3538–3550 | [Abstract](#) | [PDF \(222K\)](#)

# Interior Communication from the Subtropical to the Tropical Oceans<sup>\*</sup>

**Rui Xin Huang**

*Department of Physical Oceanography, Woods Hole Oceanographic Institution, Woods Hole, Massachusetts*

**Qi Wang**

*Physical Oceanography Laboratory, Ocean University of Qingdao, Qingdao, China*

(Manuscript received September 19, 2000, in final form May 22, 2001)

DOI: 10.1175/1520-0485(2001)031<3538:ICFTST>2.0.CO;2

### ABSTRACT

The communication from the subtropical gyre interior to the Tropics is examined using wind stress datasets and results from an ocean data assimilation system. It is shown that the interior communication can be clarified by a simple interior mass communication rate (IMCR), which can be easily calculated from the Sverdrup function. For the Northern (Southern) Hemisphere the IMCR can be defined as the meridional minimum (maximum) of the Sverdrup function maximum (minimum) at each latitude. The interior communication is closely related to the ENSO cycle, and its rate and pathway have strong interannual–decadal variability.

### 1. Introduction

Many studies on climate change have been focused on the link between the subtropics and Tropics. This link was first identified through tracer studies in 1970 and 1980. Fine and her colleagues have analyzed the tritium data and found a local tritium maximum around 140°W along the equator, which they rightly attributed to the ventilation of the subtropical water via subduction (e.g., [Fine et al. 1987](#); [McPhaden and Fine 1988](#)). This link has been discussed in many recent studies, and it has been argued that such a link can materialize in two ways, that is, a water mass formed in the subtropical basin can reach the Tropics through either an interior mass communication or via the western boundary. [Gu and Philander \(1997\)](#) proposed that such a link plays an important role in climate variability on decadal timescales.

One of the major features in wind stress near the equator is the existence of the intertropical convergence zone (ITCZ). Under the observed wind stress, the existence of the communication between the subtropics and Tropics can be seen

#### Table of Contents:

- [Introduction](#)
- [Interior communication](#)
- [Conclusions](#)
- [REFERENCES](#)
- [TABLES](#)
- [FIGURES](#)

#### Options:

- [Create Reference](#)
- [Email this Article](#)
- [Add to MyArchive](#)
- [Search AMS Glossary](#)

#### Search CrossRef for:

- [Articles Citing This Article](#)

#### Search Google Scholar for:

- [Rui Xin Huang](#)
- [Qi Wang](#)

clearly, using just a simple reduced-gravity model, as shown by [McPhaden and Fine \(1988\)](#). [Liu \(1994\)](#) studied the circulation in the subtropical–tropical regime, using a ventilated thermocline model. For a model driven under zonally mean wind stress, he concluded that communication in the lower layer between the subtropics and Tropics is possible. On the other hand, [McCreary and Lu \(1994\)](#) and [Lu and McCreary \(1995\)](#) studied the influence of the ITCZ on flow between the subtropics and Tropics and came to a different conclusion. They estimated an interior communication rate of 3 Sv, which is very close to an early estimate of 3 Sv ( $\text{Sv} \equiv 10^6 \text{ m}^3 \text{ s}^{-1}$ ) across  $10^\circ\text{N}$ , made by [Wijffels \(1993\)](#). An independent estimate inferred from the National Centers for Environmental Prediction (NCEP) data is about 2 Sv ([Liu and Huang 1998](#)). In a recent study, [Huang and Liu \(1999\)](#) updated their estimate of the interior communication rate as 3 and 11 Sv for the North and South Pacific. In addition, Huang and Liu examined the position of the communication window in both the North and South Pacific. Their estimate of the interior communication rate seems systematically lower than estimates from other studies, but the specific reason for such difference remains unclear. The subtropical–tropical pathways have been studied in many numerical simulations (e.g., [Rothstein et al. 1998](#); [Blanke et al. 1999](#); Nonaka et al. 2000, submitted to *J. Phys. Oceanogr.*).

On the other hand, recent analysis of tracer and hydrographic data has led to a communication rate that is substantially higher. For example, [Johnson and McPhaden \(1999\)](#) estimated that this communication rate is about 5 Sv for the North Pacific and 16 Sv for the South Pacific. The communication rate in the Atlantic was estimated by [Fratantoni et al. \(2000\)](#) as 1.8 Sv for the North Atlantic and 2.1 Sv for the South Atlantic.

One outstanding feature in the subtropical–tropical ocean is the positive Ekman pumping area within the ITCZ (or the South Pacific convergence zone in the South Pacific). The existence of a positive Ekman pumping rate gives rise to a small cyclonic gyre in the equatorial ocean, and it is rather strong near the eastern boundary. In addition, there might be a second cyclonic gyre near the western boundary, as indicated by the heavy dashed lines in [Fig. 1](#). Although the circulation involving the cyclonic gyres may seem complicated, it is, however, quite straightforward to deal with the case including a patch of positive Ekman upwelling within the otherwise negative Ekman pumping model ocean. If the easterlies near the equator relax, the Ekman pumping rate will become more negative, and the western boundary of the eastern cyclonic gyre extends far more westward; thus, the communication window will become narrow. If the western boundary of the eastern gyre joins with the eastern boundary of the western cyclonic gyre, the interior communication window will be closed. We will explore such possibility, using wind stress datasets and results from an oceanic data assimilation system.

In [section 2](#) we will analyze the circulation structure inferred from wind stress data in the world oceans. Although many previous studies have suggested different criteria for the interior communication rate, they are difficult to apply to the real oceans. It is our modest goal in this paper to study a simple relation between the interior mass communication rate (IMCR hereafter) and the wind stress imposed on the upper ocean. A simple index will be introduced in order to quantify the communication rate, which can be used to infer the interior communication rate from the observed wind stress alone. In addition, we will discuss the temporal variability of the IMCR and its associated pathway. Our study will be focused on the Pacific basin because this is directly related to the ENSO cycle. In addition, we will also discuss the interior communication rate and its decadal variability in the Atlantic basin. Finally, we conclude in [section 3](#).

## 2. Interior communication windows in the world oceans

We begin with the barotropic flow in the world oceans, driven by the annual Ekman pumping rate obtained from the annual mean wind stress, and we will show that an approximate rate of the communication between the subtropical gyre interior and the Tropics can be determined from the wind stress alone. Using the [Hellerman and Rosenstein \(1983\)](#) wind stress data, the Ekman pumping rate in spherical coordinates is calculated as

$$w_e = \frac{1}{r\rho_0 2\Omega \sin\phi} \left( \frac{1}{\cos\phi} \frac{\partial\tau^\phi}{\partial\lambda} - \frac{\partial\tau^\lambda}{\partial\phi} + \frac{\tau^\lambda}{\sin\phi \cos\phi} \right), \quad (1)$$

where  $r$  is the radius of the earth,  $\Omega$  is the angular velocity of the earth's rotation,  $\phi$  is the latitude,  $\lambda$  is the longitude, and  $\tau^\phi$  and  $\tau^\lambda$  are the meridional and longitudinal component of the wind stress. The meridional transport function (or the Sverdrup function) is defined as the zonal integration of the meridional mass flux within the wind-driven gyre

$$M = - \int_\lambda^{\lambda_e} hvr \cos\phi \, d\lambda = - \frac{f}{\beta} \int_\lambda^{\lambda_e} w_e r \cos\phi \, d\lambda. \quad (2)$$

where  $f = 2\Omega \sin\phi$  is the Coriolis parameter and  $\beta = r^{-1}dF/d\phi$ . Note that the meridional mass flux in a steady state is the same for either a homogeneous ocean model with a flat bottom or a reduced gravity model. The Sverdrup function is not a streamfunction because the barotropic flow includes the Ekman pumping as a source in the subtropical basin. However, the

barotropic streamlines can be identified from the pressure field. In this study we introduce a “virtual streamfunction”


$$\psi^* = \frac{f}{f_0} M = -\frac{f^2}{f_0 \beta} \int_{\lambda}^{\lambda_e} w_e r \cos \phi d\lambda, \quad (3)$$

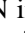
where  $f_0$  is the reference latitude where the meridional mass flux  $M$  is equal to  $\psi^*$ . Note that  $\psi^*$  is essentially the layer-integrated pressure field, and it has the same dimension as the streamfunction. Using this virtual streamfunction, the streamlines are contours with constant value of  $\psi^*$ . The mass flux between two streamlines is  $\Delta M = (f_0/f) \Delta \psi^*$ , so away from the reference latitude  $\Delta M$  is quite different from the value of  $\Delta \psi^*$ . At a latitude south of  $f_0$ ,  $\Delta M$  is larger than  $\Delta \psi^*$ . This difference is due to the fact that the Ekman pumping is downward, so it continuously adds on mass between two streamlines, thus the total mass flux between two streamlines,  $\Delta M$ , is larger than  $\Delta \psi^*$ , the total mass flux between these two streamlines at the reference latitudes.

Since the Hellerman and Rothenstein wind stress data are slightly too strong (Harrison 1989), we applied a factor of 0.8 to correct the transport function calculated. (The patterns obtained from such a calculation are, of course, independent of the choice of this correction coefficient.) Note that the volume flux here is defined as the geostrophic flow below the Ekman layer, so we will call the gyres calculated in this way the subsurface gyres because these gyres do not include the Ekman flux within the surface Ekman layer. In many classic papers discussing the wind-driven circulation, the total mass flux, including the Ekman flux, is calculated (e.g., Munk 1950). At low latitudes the mass flux in the Ekman layer flows off the equator; however, the subsurface current may flow equatorward, if the Ekman pumping rate is negative. Thus, the barotropic meridional transport function based on the total mass flux does not represent the subsurface meridional flow correctly. Even if the Ekman pumping rate is positive, the barotropic transport function based on the total mass flux tends to have a cyclonic gyre in the Tropics, which has poleward mass flux stronger than that calculated from the definition used in this study.

In many previous studies, the communication between the subtropics and Tropics has been discussed in terms of potential vorticity contours in the subsurface layers. The pathway and the blockage of the communication have been interpreted in terms of the high potential vorticity ridge in the eastern basin (e.g., Lu and McCreary 1995; Johnson and McPhaden 1999). The high potential vorticity ridge in the eastern basin is directly related to the positive Ekman pumping rate there; thus, it is more straightforward to link the interior communication with the barotropic Sverdrup function and the cyclonic gyre associated with the Ekman upwelling prevailing in the ITCZ, especially near the eastern boundary.

#### a. A simple index for the IMCR

As discussed above, the cyclonic gyres at the latitudes of the ITCZ are defined by the subsurface geostrophic mass flux, excluding the poleward Ekman flux in the surface layer; thus, they are much weaker than the cyclonic gyres calculated from the total volume flux (including the Ekman flux). Most importantly, the cyclonic gyres from those classic studies block the interior passage between the subtropics and Tropics, but the subsurface cyclonic gyres, as shown in Fig. 2 , do not entirely block the interior communication between the subtropical gyre and the Tropics.

For the annual mean flow field, there is a window in the middle or the western basin that allows the interior communication between the subtropics and Tropics. Note that there might be two small cyclonic gyres at the latitude of the ITCZ, one near the eastern boundary and one near the western boundary, as shown in Fig. 2  around 9°N in the Pacific Ocean. Simply taking the meridional minimum of the Sverdrup function value at the western boundary may miss the communication window in the middle basin. Thus, for the Northern Hemisphere, we propose the following quantity as the IMCR

$$I_c = \max[0, \min_y(\max_x M)]. \quad (4)$$

First, the maximum of  $M$  at each latitude gives the maximum equatorward mass flux at that latitude; second, taking the meridional minimum of this maximum (typically searching for the maximum between 5° and 20° off the equator) gives the mass flux through the choke latitude of the basin. Note that IMCR defined in this way is nonnegative. The corresponding IMCR for the southern oceans is defined similarly:

$$I_c = -\min[0, \max_y(\min_x M)]. \quad (5)$$

Since the Sverdrup function is defined in terms of the Ekman pumping rate, this index is directly related to subduction in the subtropical basin. Thus, the IMCR defined above is a large-scale wind-stress-related index that indicates the equatorward mass flux due to subduction in the subtropical gyre interior and its subsequent equatorward flow.

## b. The climatological mean circulation

The wind-driven circulation has quite different structure in the two hemispheres. In fact, the cyclonic tropical gyre near the western coast of South America is very weak, and its effect on the basin-scale circulation is almost negligible; thus, the interior communication in the South Pacific is totally unblocked. The cyclonic tropical gyre in the South Atlantic is also weak, and thus the interior communication is largely free.

On the other hand, the cyclonic gyre in the south Indian Ocean extends all the way to the western boundary of the basin, so there is no interior communication between the subtropics and Tropics. Therefore, the equatorial currents in the south Indian Ocean have no direct connection with the subtropical gyre interior. This may imply some special character of the equatorial thermocline; however, this is left for future study.

The IMCR for the Pacific has been estimated as  $5 \pm 2$  Sv (at  $8^\circ\text{N}$ ) for the Northern Hemisphere and  $16 \pm 2$  Sv (at  $8^\circ\text{S}$ ) for the Southern Hemisphere (Johnson and McPhaden 1999). From the Florida State University (FSU) wind stress data, we obtained the IMCR averaged between 1961 and 1999 as 5.84 Sv for the Northern Hemisphere and 27.05 Sv for the Southern Hemisphere (Table 1). (The Hellerman and Rosenstein wind stress data, after applying a factor of 0.8, give 4.56 Sv for the North Pacific, and 19.16 Sv for the South Pacific.) The difference between these estimates may be due to errors in wind stress data and the existence of the meridional overturning cell in the Pacific. Note that Johnson and McPhaden (1999) used a reference level of 900 dbar. Thus, if a different reference level were used, their estimate may change. In any case, these estimates of IMCR for the Pacific seem to be roughly consistent with each other. Most interestingly, the equatorward mass communication in the Pacific is dominated by the source from the Southern Hemisphere.

The IMCR for the Atlantic is about a quarter of that for the Pacific, and this is primarily due to the smaller size of the basin. Fratantoni et al. (2000) estimated that the mass transport in the upper ocean in the Atlantic is 10.9 Sv. Since this flux includes the flux within the western boundary current, it is different from the IMCR discussed in this note. The flux numbers quoted here are for the thermocline layers 2 and 3 and intermediate layers 4 and 5 in their analysis, which are defined as between  $\sigma_t = 25.2$  and 27.55, corresponding to a rest depth of 60–1080 m.

Furthermore, the meridional thermohaline cell in the Atlantic is much stronger than that in the Pacific; thus, our estimates, based on the wind-driven circulation theory alone, may not provide a practical value for the IMCR. The Trenberth et al. (1989) climatological wind stress data were also used to estimate the IMCR for both the Pacific and Atlantic; however, the results are quite different from that obtained from other datasets, with the IMCR equal to 3.54 Sv and 5.62 Sv in the North and South Pacific and 2.85 Sv and 7.17 Sv in the North and South Atlantic, respectively. Note that the Trenberth et al. (1989) dataset is based on reanalysis of atmospheric data, and are known for their inaccuracy for the low-latitude wind over the Tropics; thus, the IMCR calculated from these wind stress datasets may not be very reliable.

As discussed above, the Sverdrup function is not a streamfunction for the subsurface geostrophic flow, and the exact shape of the communication window should be inferred from the streamlines of the barotropic flow. Using the virtual streamfunction introduced above, we can identify the interior communication window clearly; see Fig. 3. For both the North Pacific and North Atlantic the communication window is a narrow passage wound around the western edge of the cyclonic gyre and the eastern boundary. The center of the communication window in the North Pacific is near  $170^\circ\text{E}$  at  $9^\circ\text{N}$ , and it is  $120^\circ\text{W}$  near the equator. In particular, these pathways move eastward south of the choke latitudes. Of course, within the vicinity of the equator, other dynamic processes must be taken into consideration, such as the inertial terms and mixing term (e.g., Huang and Pedlosky 2000).

However, a close examination reveals that the location of the communication pathway near the equator is about  $20^\circ$  west of the tritium maximum as identified from observations by Fine et al. (1987). On the other hand, the location of the pathway center at  $9^\circ\text{N}$  is very close to that identified from the tritium data, as will be shown shortly. The mismatch in the location of the tritium maximum and the communication pathway inferred from the climatological wind is puzzling. Liu and Huang (1998) tried to explain this mismatch. One possible mechanism, which they suggested, is that the Mindanao eddy may induce an eastward current north of the equator that brings about the westward shift of the tritium maximum, as observed from data. However, this mismatch may well be due to the decadal variability of the communication window, as will be discussed shortly.

The communication window in the North Atlantic is rather narrow, as seen in Fig. 3b. Thus, the interior connection between the subtropics and Tropics is relatively weak, and decadal climate signals that can pass through this choke latitude and propagate to the equator may be relatively weak too.

The communication pathways in the Southern Hemisphere are structurally quite different; see the lower parts of Figs. 3a and 3b. In both the South Pacific and South Atlantic, the communication pathway moves northwestward, without much winding around the cyclonic gyre in the eastern basin. The different features of the pathway in the two hemispheres are clearly related to the asymmetric nature of the wind stress pattern in the two hemispheres. In contrast to the ITCZ in the North Pacific and North Atlantic, the corresponding structure of the subtropical–tropical atmospheric circulation in the



Southern Hemisphere is quite different. For example, the South Pacific convergence zone appears in the South Pacific and is slanted.

As discussed above, in the North Pacific and North Atlantic, the interior communication window appears as a narrow corridor wound around the western edge of the cyclonic gyre in the eastern boundary, and it extends poleward along the eastern boundary of the basin. Thus, the interior communication in the Northern Hemisphere basins affects the eastern part of the equatorial thermocline, but with virtually no effect on the western part of the equatorial thermocline. On the other hand, the interior communication windows in the South Pacific and South Atlantic open up over the whole width of the basin, so changes in extratropics can be transported toward the equator and affect the thermocline there. This asymmetry of the interior communication windows may give rise to some important dynamic consequence for the structure of the equatorial thermocline and its decadal variability; however, this is left for further study.

Recall contours of virtual streamfunction indicate the streamlines only and the mass flux within the pathways can be calculated by  $\Delta M = f^{-1}/f_0 \Delta \psi^*$ , shown by the heavy lines in Fig. 4 for the Pacific and Atlantic, while the maximal meridional mass flux at the corresponding latitude is indicated by the thin line. (For the Northern Hemisphere, the communication window is at the latitude where the meridional mass flux is minimum.) Note that the total mass flux within the communication window declines poleward from the choke latitude, but it increases equatorward. This meridional change in the mass flux is due to the contribution of Ekman pumping. For example, in the North Pacific, the total mass flux within the communication pathway increases from 4.56 Sv at the choke latitude (9°N) to 13.6 Sv at 3°N; in the South Pacific, the total mass flux within the communication passage increases from 19.16 Sv at the choke latitude (13°S) to 82.37 Sv at 3°S. Such an increase in mass flux comes from the local Ekman pumping. Combined with the off-equator Ekman flux, this mass flux increment consists of the equatorward branch of the local meridional overturning cell.

It is also interesting to note that some streamlines within the communication passage may not actually reach the equator directly. In fact, in the Southern Hemisphere some of these streamlines may hit the western boundary before it reaches the equator, as shown in Fig. 3. The flux that actually reaches the equator is depicted by the thin dashed line in Fig. 4c, and the corresponding streamline in the South Atlantic is depicted by the short heavy line in Fig. 4d.

Assuming climate variability has small amplitude, then these passages should serve as the pathways for climate variability in the thermocline. However, as will be shown shortly, climate variability on decadal timescales may be so strong that the passage itself may change over decadal timescales, and the corresponding pathways of temperature and salinity anomalies may be different from their climatological mean.

### c. Interannual–decadal variability of IMCR

It is important to note that the index introduced above is a *barotropic index*; its meaning requires careful interpretation. First, this index shows the barotropic mass flow in an ocean with a flat bottom (here we neglect the bottom friction). Since the barotropic flow in a basin can adjust to changes in the wind stress within a few days, monthly mean wind stress can be used to infer variability in the barotropic circulation. Second, for a time period longer than the time for the first baroclinic Rossby waves to cross the basin, the circulation structure in terms of the first baroclinic mode is established; thus, this barotropic index can also be used as the first baroclinic index to infer changes in the wind-driven circulation above the main thermocline.

The group velocity of the first baroclinic Rossby wave is  $C_{gx} = \beta \lambda^2$ , where  $\lambda = (g' D)^{1/2}/f$  is the radius of deformation,  $\beta = 2\Omega \cos \phi/R$ , and  $f = 2\Omega \sin \phi$ . Assuming the basin is 140° wide in the zonal direction, and the reduced gravity for the main thermocline is  $g' = 3 \text{ cm s}^{-2}$ , the corresponding time for the first baroclinic Rossby waves to travel across the basin at low latitudes is much shorter than that at midlatitudes. As discussed above, the choke latitude in the North Pacific is at 9°N where the adjustment time for the main thermocline is less than 2 years. Thus, the interannual variability of the interior mass communication rate can be inferred from wind stress average over a couple of years. The corresponding adjustment time for the Atlantic is less than one year because the Atlantic basin is less than 70° wide.

As discussed above, although the adjustment time is much longer at higher latitudes, the fast adjustment process around the choke latitude implies that the interior mass communication rate between the subtropics and Tropics can be diagnosed from wind stress data with a multiyear low-pass filter. (From Fig. 3, one notices that at higher latitudes the pathway is very close to the eastern boundary, so the adjustment time is as short as that for the low latitudes. Thus, the whole communication pathway can be established within no more than two years.) Note that wind stress at  $t = t_0$  cannot affect the circulation for  $t < t_0$ ; that is, the mass flux rate is controlled by the wind stress before and up to the current year. Thus, the three-year low-pass filtering in time used in our study of the Pacific is defined as

$$\bar{I}_c = (I_{c,0} + I_{c,-1} + I_{c,-2})/3,$$

where the subscript  $-1$  and  $-2$  indicate the year before and two years before.

This method was applied to several wind stress datasets: the Florida State University wind stress data ([Legler and O'Brien 1988](#), FSUW hereafter), the Da Silva wind stress dataset ([Da Silva et al. 1994](#), DASW hereafter), and the wind stress from the NCEP reanalysis ([Kalnay et al. 1996](#), NCEPW hereafter).

In addition, we have analyzed the circulation obtained from the NCEP Ocean Data Analysis System ([Ji et al. 1995](#); [Behringer et al. 1998](#); [Worley 1996](#); NCEPO hereafter). The NCEPO is based on a combination of the Modular Ocean Model (MOM) developed at Geophysical Fluid Dynamical Laboratory and the variational data assimilation method of [Derber and Rosati \(1989\)](#). The model is driven by the climatological mean annual cycle of wind stress of [Hellerman and Rosenstein \(1983\)](#) combined with monthly anomalies derived from the pseudostress fields of the FSUW ([Legler and O'Brien 1988](#)). The climatological annual cycle of [Oberhuber \(1988\)](#) and the annual cycle of sea surface salinity from [Levitus and Boyer \(1994\)](#) were used as the heat flux and salinity relaxation condition, respectively. A most important aspect of the analysis includes assimilation of many available in-situ observations, such as XBTs and the Thermal Array in the Ocean (TAO) array of moored buoys, and the monthly SST analysis of [Reynolds and Smith \(1994\)](#).

The NCEPO dataset includes all the necessary information about the circulation, so streamfunction maps on different isopycnal layers can be reconstructed accordingly. Our reconstruction of streamfunction maps showed circulation quite similar to that obtained from the wind stress datasets. Thus, these streamfunction maps are not repeated here, and we will concentrate on the vertically integrated mass flux from the subtropical to equatorial ocean. In the present case the vertically integrated equatorward volume flux below the Ekman layer is defined as

$$M = - \int_{\lambda}^{\lambda_e} r \cos \phi \, d\lambda \left( \int_{\rho_b}^{\rho_s} h_{\rho} \mathbf{v} \, d\rho - \tau^x / \rho_0 f \right),$$

where  $h_{\rho}$  and  $\mathbf{v}$  are the thickness and meridional velocity of each isopycnal layer, and  $\rho_s$  and  $\rho_b$  are the density at the sea surface and the lower moving layer. The IMCR is calculated according to the definition discussed above, using the integrated volume flux  $M$  defined above. It is found that the IMCR calculated in this way is insensitive to the specific choice of the density of the lower boundary,  $\rho_b$ , as long as it is deep enough, and results presented here are based on  $\sigma_b = 27.5$ .

For the North Pacific the diagnosis based on the FSUW suggests that the IMCR was quite high during the 1970s, which may be associated with the anomalous condition in the atmospheric circulation at that time period. Moving further backward in time, the IMCR was much lower in the 1960s. For the time period when both FSUW and NCEPO overlap, IMCR calculated from FSUW and NCEPO are similar, with the IMCR from FSUW noticeably smaller, [Fig. 5a](#). They both indicate a strong IMCR during 1984–85 and 1989–90, but there is a strong decline in IMCR during early 1990. The results from FSUW suggests a complete shutdown of the interior communication; while the results from NCEPO indicate a substantial reduction of IMCR.

The results from the DASW are in general agreement with these two analyses discussed above. There are three high IMCR periods, that is, 1950s, 1970s, and 1980s. There is also a clear trend of rapid decline during the early 1990s, consistent with the results from the other two datasets.

The IMCR diagnosed from the NCEPW data is very small and close to zero for most of the time. Such a small IMCR is in contradiction with observation evidence as discussed by [Fine et al. \(1987\)](#) and [Johnson and McPhaden \(1999\)](#). It is thus speculated that the NCEPW is not suitable as a forcing field in the study of the interior communication in a direct oceanic circulation simulation.

As discussed above, IMCR diagnosed from NCEPO is very similar to that diagnosed from FSUW with the highs and lows in these two calculations in phase, but the IMCR calculated from NCEPO is systematically larger than that from FSUW. The similarity of these two results indicate that the IMCR is primarily dominated by the barotropic circulation driven by the wind stress curl, with the baroclinic structure playing a minor role. Recall that the FSUW wind stress dataset was used in both of these two models, so the differences between these two cases are due to either the thermohaline circulation or the data assimilation component in NCEPO. In particular, the southward return flow of the thermohaline cell in the upper ocean may be the major contributor of the systematic difference between the IMCR calculated from FSUW and NCEPO. In addition, the NCEPO includes the contribution from in situ subsurface observations; thus even under imperfect wind stress data or model, the circulation obtained from the data assimilation model can match that of the real ocean.

Note that our results here are noticeably different from those of [Huang and Liu \(1999\)](#). This may be due to the fact that NCEPO has been improved substantially over the past few years, as discussed in the most recent publication by [Behringer et al. \(1998\)](#). As a result, the IMCR we obtained from NCEPO is much larger than the 3 Sv reported by [Huang and Liu \(1999\)](#),

who apparently used an early version of the data from the NCEP Ocean Data Analysis System.

IMCR in the South Pacific, diagnosed from FSUW, increased gradually from 1961 to 1975, and decreased afterward. It reached a minimum around 1984, then went up again, and reached a maximum in 1997. Most interestingly, the IMCR for the South Pacific seemed to reach a historic low after the recent ENSO cycle of 1997–99, which is also one of the strongest ENSO events in the instrumented record. For the South Pacific the IMCR diagnosed from both FSUW and NCEPO is similar. There are two periods, around 1984 and 1998, when the IMCR is much smaller than the climatological mean. The DASW gives rise to a relatively flat rate over the past 50 years, with a gradual increase. The NCEPW in the South Pacific gives a very small and ever declining IMCR over the past 40 years. Such a small IMCR is again a major discrepancy with the observation studies cited above.

Note that IMCR can be very sensitive to the structure details of the wind stress data because the window is relatively narrow. Thus, small errors in the vicinity of the communication window can induce a relatively large error in IMCR. The NCEP reanalysis was done based on the 1995 version of the operational global atmospheric model, and the winds are too weak in the tropical Pacific region (Ming Ji 2000, personal communication). Therefore, the NCEP Ocean Data Analytical System is based on a combination of the FSU wind stress data, plus some other available data, but not the NCEP wind.

The IMCR and its decadal variability in the Atlantic Ocean is studied using three wind stress datasets: the FSUW, the NCEPW, and the Servain et al. wind (Servain et al. 1987; the data is currently available online at <http://www.coaps.fsu.edu/WOCE/SAC/>; SACW hereafter). The IMCR in the Atlantic is relatively small (Fig. 6). In the North Atlantic, the IMCR is typically within 2–5 Sv, with the exception for the results obtained from the SACW. It is noted that there is a very strong meridional overturning cell in the Atlantic, and this cell can certainly affect the interior communication.

For the South Atlantic, the IMCR is slightly larger than that for the North Atlantic, ranging from 3 to 6 Sv. Although all three wind stress datasets give similar IMCR for the 1970s and early 1980s, the NCEPW gives much smaller IMCR for the 1990s. Recall that NCEPW has a rather disappointing performance for the Pacific, it is thus concluded, tentatively, that IMCR has a general upward trend in the 1990s, as indicated by the heavy dashed line (SACW) and the thin solid line (DASW).

#### *d. Seasonal cycle of IMCR*

With the results from NCEPO, we can examine the time evolution of the communication window in details, Fig. 7. There is clearly very strong annual and interannual variability of IMCR. Most importantly, this dataset allows us to analyze the seasonal cycle of the IMCR, depicted as the heavy solid lines in Fig. 8. It is interesting to note that in the North Pacific the IMCR has a very strong seasonal cycle, high in the winter and spring (a maximum of 18 Sv in March) and low in the summer and fall (a minimum of 3.7 Sv in September).

The simple index discussed above cannot apply to the case of seasonal cycle. Recall that our index is based on the Sverdrup relation for the quasi-steady wind-driven circulation. The Sverdrup relation is valid only for the timescale longer than the time for the first baroclinic Rossby waves to move across the basin. As the Rossby waves move westward, they leave behind a wind-driven circulation that is mostly confined above the main thermocline, with the abyssal water essentially motionless. For a seasonal cycle, the Sverdrup relation does not apply, so our index cannot be used to diagnose the IMCR for such short timescales.

The deviation from the monthly mean cycle is very strong, Fig. 9. In general, IMCR is high between major El Niño events and low during the El Niño. The 1997–98 event is very special because the IMCR in both the North and South Pacific was quite high just before the El Niño phase, but they both declined sharply during the El Niño phase. We speculate that this very special feature may related to other special features of this strong ENSO event; however, this is left for further study.

#### *e. Decadal shift of the communication window*

The communication window and the associated pathway itself varies greatly over a decadal timescale, especially in the North Pacific, shown in Fig. 10 by two sections taken along 9 and 3°N. As identified from the FSUW, the window at 9° N, roughly the choking latitude, was relatively narrow in the mid-1960s and then expanded in the 1970s. However, the window started to diminish from the middle of the 1970s and became completely closed in the 1990s. In the equatorial regime, the window is located in a more eastward zonal location, as shown by the 3°N section in Fig. 10. Note that the location of the window also migrates during the past three decades. In the mid-1960s the window was centered around 120° W, but it moves westward during the 1970s, then moves eastward during the 1980s. The zonal migration of the window identified from the wind stress is consistent with the migration of the tracer maximum identified from in situ observations.

For example, the communication window was much wider than normal during the period of 1973–76. Close to the equator the center of the window was around 140°W, which is consistent with the position of the tritium maximum along

the equator as identified from the tritium data collected during the period of 1973–82 by [Fine et al. \(1987\)](#). Thus, the mismatch between the tritium maximum along the equator and the center of the pathway near the equator may be due to the decadal variability of the wind stress.

The communication pathway for the South Pacific also went through similar decadal variability, with peaks appearing during 1973–76 and 1993–97, closely related to the strong ENSO cycles at those times. On the other hand, the southern passage was relatively narrow for the periods of 1965–68 and 1985–88, figures not included.

The time evolution of the communication window is best diagnosed from NCEPO, [Fig. 11](#). The width and the location of the window is clearly related to the ENSO cycle. Before each ENSO event, the strong easterlies induce strong Ekman pumping, and thus a large interior communication window and strong equatorward mass flux. During the ENSO phase, the easterlies substantially weaken, and thus the associated weakened easterlies give rise to small interior communication window and weak equatorward mass flux. The communication window for the North Pacific was substantially narrow in the early 1990s, but nevertheless it was still open. This is probably the most noticeable difference between results from FSUW and NCEPO.

The IMCR defined above is closely related to the strength of the easterlies at the equator. This relation is shown in [Fig. 12](#), where the IMCR is plotted side by side with the zonal mean of the easterly along the equator, which is rescaled  $\tau^* = -50(\tau^x - \bar{\tau}^x + 0.1)$ ,  $\tau^x$  is in unit of  $\text{dyn cm}^{-2}$ . During the 1970s and 1980s there is a strong correlation between the IMCR and the easterlies along the equator, that is, strong easterlies induces strong interior communication in the North Pacific. Such correlation is, however, absent before 1972 and after 1994. The reason for such noncorrelation remains unclear at this time, and it is left for further study.

### 3. Conclusions

The interior mass communication between the subtropics and Tropics is fed by subduction in the subtropical gyre interior and the subsequent equatorward flow. Most importantly, the interior communication between the subtropics and Tropics can be quantified in terms of a simple index derived from the choke value of the Sverdrup function, defined as the zonally integrated meridional mass flux. In the Pacific Ocean, the climatological mean of the interior mass communication is about 30 Sv, which consists of a substantial fraction of the mass flux in the equatorial undercurrent; thus, interior communication plays a vital role in the dynamic balance of the equatorial thermocline.

In the North Pacific and North Atlantic, the interior communication windows appear as a narrow corridor winding around the western edge of the cyclonic gyre in the eastern boundary, and it extends poleward along the eastern boundary of the basin. Thus, the interior communication in the Northern Hemisphere basins affects the eastern part of the equatorial thermocline, but with virtually no effect on the western part of the equatorial thermocline. On the other hand, the interior communication windows in the South Pacific and South Atlantic open up over the whole width of the basin, so changes in the extratropics can be transported toward the equator and affect the thermocline there.

Over the past 40 years, this index went through major changes that are closely related to the ENSO cycles in the ocean. Furthermore, there are clear signs of decadal variability in this index, which may indicate some subtle changes in the communication between the subtropics and Tropics. Such changes can certainly bring substantial changes in the structure of the thermocline along the equator, and thus affect the ENSO cycle there. Since this index is defined in terms of the barotropic mass flux, it does not include the complete information regarding the vertical structure of the pathway associated with such an interior communication. Thus, further study is needed in order to explore its contribution to the dynamics of the equatorial system.

In addition, this index is derived from a purely wind-driven circulation theory, so it requires some modification in order to include the effects of other dynamic processes, such as the thermohaline circulation. Because the thermohaline circulation in the Atlantic is rather strong, the direct application of this index to the Atlantic should be made with caution. On the other hand, the thermohaline cell in the Pacific is relatively weak; thus, the IMCR index proposed here can be a useful tool in diagnosing the dynamics that sets up the equatorial thermocline in the Pacific, especially its link with the subtropical thermocline.

Results obtained from NCEPO indicated that the IMCR is primarily controlled by the barotropic circulation driven by the wind stress curl for a timescale from interannual to decadal. Thus, the IMCR inferred from the wind stress curl can be used as a useful index for interpreting the decadal variability of the interior communication between the extratropics and Tropics. This barotropic index can be used to explain the difference in IMCR and the pathways obtained from numerical simulation of the oceanic circulation based on different wind stress datasets.

The communication between the subtropical and tropical oceans can also go through other channels, such as the western or the eastern boundary currents in the oceans. The situation in the Pacific Ocean is even more complicated because the existence of the Indonesian Throughflow and western boundary currents, such as the Mindanao Current. A comprehensive



## Acknowledgments

RXH was supported by the National Science Foundation through Grant OCE-9616950 and by NOAA through Grant NA36GP0460 to the Woods Hole Oceanographic Institution. QW was supported by the Advanced Visiting Scholar Program of the Chinese Academy of Sciences through Grant KZCX2-205; QW acknowledges many constructive suggestions and help from Dr. Qinyu Liu.

---

## REFERENCES

- Behringer D. W., M. Ji, and A. Leetmaa, 1998: An improved coupled model for ENSO prediction and implication for ocean initialization. Part I: The ocean data assimilation system. *Mon. Wea. Rev.*, **126**, 1013–1021. [Find this article online](#)
- Blanke B., M. Arhan, G. Madec, and S. Roche, 1999: Warm water paths in the equatorial Atlantic as diagnosed with a general circulation model. *J. Phys. Oceanogr.*, **29**, 2753–2768. [Find this article online](#)
- Da Silva A. M., C. C. Young, and S. Levitus, 1994: *Atlas of Surface Marine Data 1994*. Vol. 1: *Algorithms and Procedures*, U. S. Dept. of Commerce, 83 pp.
- Derber J. D., and A. Rosati, 1989: A global oceanic data assimilation system. *J. Phys. Oceanogr.*, **19**, 1333–1347. [Find this article online](#)
- Fine R. A., W. H. Peterson, and H. G. Ostlund, 1987: The penetration of tritium into the tropical Pacific. *J. Phys. Oceanogr.*, **17**, 553–564. [Find this article online](#)
- Fratantoni D. M., W. E. Johns, T. L. Townsend, and H. E. Hurlburt, 2000: Low-latitude circulation and mass transport pathways in a model of the tropical Atlantic Ocean. *J. Phys. Oceanogr.*, **30**, 1944–1966. [Find this article online](#)
- Gu D., and S. G. Philander, 1997: Interdecadal climate fluctuations that depend on exchanges between the Tropics and extratropics. *Science*, **275**, 805–807. [Find this article online](#)
- Harrison D. E., 1989: On climatological mean wind stress and wind stress curl fields over the World Ocean. *J. Climate*, **2**, 57–70. [Find this article online](#)
- Hellerman S., and M. Rosenstein, 1983: Normal monthly wind stress over the world ocean with error estimates. *J. Phys. Oceanogr.*, **13**, 1093–1104. [Find this article online](#)
- Huang B., and Z. Liu, 1999: Pacific subtropical–tropical thermocline water exchange in the National Centers for Environmental Prediction ocean model. *J. Geophys. Res.*, **104**, 11065–11076. [Find this article online](#)
- Huang R. X., and J. Pedlosky, 2000: Climate variability of the equatorial thermocline inferred from a two-moving layer model of the ventilated thermocline. *J. Phys. Oceanogr.*, **30**, 2610–2626. [Find this article online](#)
- Ji M., A. Leetmaa, and J. Derber, 1995: An ocean analysis system for seasonal to interannual climate studies. *Mon. Wea. Rev.*, **123**, 460–481. [Find this article online](#)
- Johnson G. C., and M. J. McPhaden, 1999: Interior pycnocline flow from the subtropical to the equatorial Pacific Ocean. *J. Phys. Oceanogr.*, **29**, 3073–3089. [Find this article online](#)
- Kalnay E., and Coauthors., 1996: The NCEP/NCAR 40-Year Reanalysis Project. *Bull. Amer. Meteor. Soc.*, **77**, 437–472. [Find this article online](#)
- Legler D. M., 1988: *Tropical Pacific Wind Stress Analysis for TOGA, IOC Time Series of Ocean Measurements*. IOC Technical Series 33, Vol. 4, UNESCO.
- Levitus S., and T. P. Boyer, 1994: *World Ocean Atlas 1994*. Vol. 4: *Temperature* NOAA Atlas NESDIS 4. 117 pp.
- Liu Z., 1994: A simple model of the mass exchange between the subtropical and tropical ocean. *J. Phys. Oceanogr.*, **24**, 1153–1165. [Find this article online](#)
- Liu Z., and B. Huang, 1998: Why is there a tritium maximum in the central equatorial Pacific thermocline? *J. Phys. Oceanogr.*, **28**, 1527–1533. [Find this article online](#)
- Lu P., and J. P. McCreary, 1995: Influence of the ITCZ on the flow of the thermocline water from the subtropical to the equatorial Pacific

McCreary J. P., and P. Lu, 1994: Interaction between the subtropical and equatorial ocean circulation: The subtropical cell. *J. Phys. Oceanogr.*, **24**, 466–497. [Find this article online](#)

McPhaden M. J., and R. A. Fine, 1988: A dynamical interpretation of the tritium maximum in the Central Equatorial Pacific. *J. Phys. Oceanogr.*, **18**, 1454–1457. [Find this article online](#)

Meyers S. D., J. J. O'Brien, and E. Thelin, 1999: Reconstruction of monthly SST in the Tropical Pacific Ocean during 1968–1993 using adaptive climate basis functions. *Mon. Wea. Rev.*, **127**, 1599–1612. [Find this article online](#)

Munk W. H., 1950: On the wind-driven ocean circulation. *J. Meteor.*, **7**, 79–93. [Find this article online](#)

Oberhuber J. M., 1988: An atlas based on “COADS” data set. Tech. Rep. 15, Max-Planck-Institut für Meteorologie.

Reynolds R. W., and T. M. Smith, 1994: Improved global sea surface temperature analysis using optimum interpolation. *J. Climate*, **7**, 929–948. [Find this article online](#)

Rothstein L. M., R.-H. Zhang, A. J. Busalacchi, and D. Chen, 1998: A numerical simulation of the mean water pathways in the subtropical and tropical Pacific Ocean. *J. Phys. Oceanogr.*, **28**, 322–343. [Find this article online](#)

Servain J., M. Seva, S. Lukas, and G. Rougier, 1987: Climate atlas of the tropical Atlantic wind stress and sea surface temperature: 1980–1984. *Ocean Air Inter. J.*, **1**, 109–182.

Trenberth K., J. Olson, and W. Large, 1989: A global ocean wind stress climatology based on ECMWF analyses. National Center for Atmospheric Research, Tech. Rep. NCAR/TN-338+STR, 93 pp.

Wijffles S., 1993: Exchanges between hemisphere and gyres: A direct approach to the mean circulation of the equatorial Pacific. Ph.D. thesis, Woods Hole Oceanographic Institution, Massachusetts Institute of Technology, 267 pp.

Worley S., 1996: NCEP ODAS tropical Pacific Ocean analysis. Data Supporting Section Scientific Computing Division, NCAR, DS277.1.

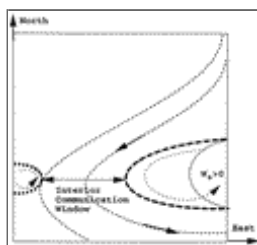
## Tables

TABLE 1. Interior mass communication rate in the world oceans, in Sv, where HRW: Hellerman and Rosenstein wind stress data (1983), DASW: Da Silva et al. (1994) wind stress data, SACW: Servain et al. (1987) wind stress data, FJDH: Fratantoni et al. (2000), FSUW: the Florida State University wind stress data (Legler and O'Brien 1988), NCEPO: NCEP Ocean Data Analysis System (Ji et al. 1995), and JM: Johnson and McPhaden (1999)

Data	Basin									
	Atlantic				Pacific				Indian	
	HRW	DASW	SACW	FJDH	HRW	DASW	FSUW	NCEPO	JM	HRW
NH	1.28	3.31	1.46	1.8	4.56	9.44	5.88	9.46	5 ± 2	7
SH	5.18	4.65	5.09	2.1	19.16	12.35	17.05	24.12	16 ± 2	0.0
Total	6.46	7.96	6.55	3.9	23.72	26.79	22.93	33.58	21 ± 4	0.0

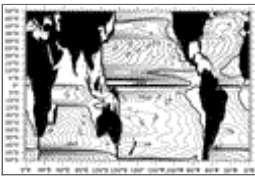
[Click on thumbnail for full-sized image.](#)

## Figures



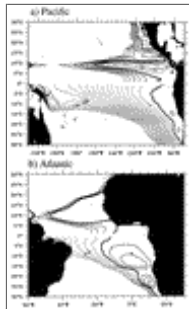
[Click on thumbnail for full-sized image.](#)

FIG. 1. Sketch of the interior communication window in the subtropical–tropical regime, including two cyclonic gyres near the eastern and western boundaries



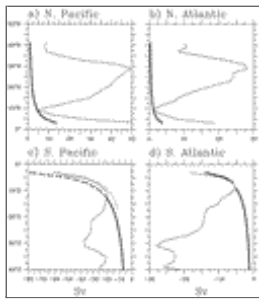
[Click on thumbnail for full-sized image.](#)

FIG. 2. Annual mean barotropic meridional mass flux, in Sv, below the Ekman layer based on the Hellerman and Rosenstein wind stress data



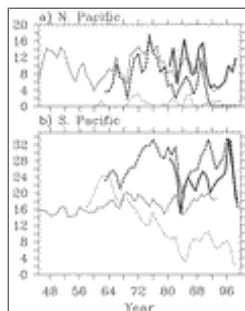
[Click on thumbnail for full-sized image.](#)

FIG. 3. Interior communication window identified from the virtual streamfunction (in Sv) in (a) Pacific and (b) Atlantic



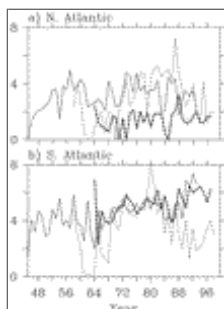
[Click on thumbnail for full-sized image.](#)

FIG. 4. Meridional profiles for the mass flux in the interior communication windows (heavy lines) and the wind-driven gyres (thin lines), in Sv



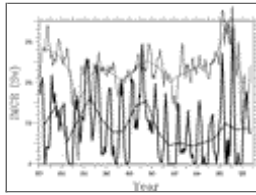
[Click on thumbnail for full-sized image.](#)

FIG. 5. The annual mean IMCR for the Pacific Ocean. The heavy solid line is based on NCEPO; the heavy dashed line is based on the FSUW; the thin solid line is based on the DASW; the thin dashed line is based on the NCEPW



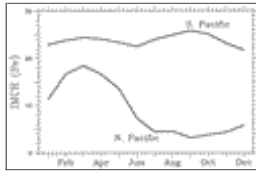
[Click on thumbnail for full-sized image.](#)

FIG. 6. The annual mean IMCR for the Atlantic Ocean. The heavy dashed line is based on the SACW; the thin solid line is based on the DASW; the thin dashed line is based on the NCEPW



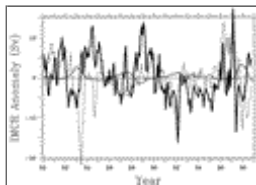
[Click on thumbnail for full-sized image.](#)

FIG. 7. IMCR diagnosed from the NCEPO: the heavy solid line is the monthly mean for the North Pacific, and the heavy dashed line is the annual mean. The thin solid line is the monthly mean for the South Pacific, and the thin dashed line is the annual mean



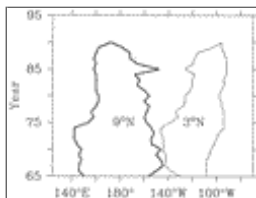
[Click on thumbnail for full-sized image.](#)

FIG. 8. The seasonal cycle of the IMCR, diagnosed from NCEPO



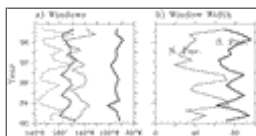
[Click on thumbnail for full-sized image.](#)

FIG. 9. Deviation of IMCR from the monthly mean: the heavy solid line is for the North Pacific, the thin dashed line for the South Pacific, and the solid thin line is the ENSO index (which is a 5-month running mean of spatially averaged SST anomalies over the tropical Pacific: 4°S–4°N, 150°–90°W; [Meyers et al. 1999](#))



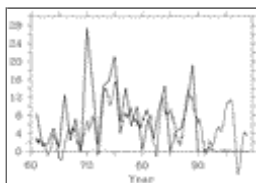
[Click on thumbnail for full-sized image.](#)

FIG. 10. The zonal location of the interior communication window at 9° and 3°N, identified from the FSU wind stress data



[Click on thumbnail for full-sized image.](#)

FIG. 11. (a) The zonal location of the interior communication window, identified from the data assimilation: the thin lines for the North Pacific, and the heavy lines for the South Pacific; the solid lines indicate the eastern edge, and the dashed lines indicate the western edge. (b) The width of the window



[Click on thumbnail for full-sized image.](#)

FIG. 12. The relation between the annual IMCR in the North Pacific (solid line, diagnosed from the FSU wind stress data) and the strength of the easterly (rescaled) along the equator and at the middle of the basin (dashed line)



\* Woods Hole Oceanographic Institution Contribution Number 10262.

*Corresponding author address:* Dr. Rui Xin Huang, Department of Physical Oceanography, Woods Hole Oceanographic Institution, Woods Hole, MA 02543. E-mail: [rhuang@whoi.edu](mailto:rhuang@whoi.edu)

top ▲



© 2008 American Meteorological Society [Privacy Policy and Disclaimer](#)

Headquarters: 45 Beacon Street Boston, MA 02108-3693

DC Office: 1120 G Street, NW, Suite 800 Washington DC, 20005-3826

[amsinfo@ametsoc.org](mailto:amsinfo@ametsoc.org) Phone: 617-227-2425 Fax: 617-742-8718

[Allen Press, Inc.](#) assists in the online publication of *AMS* journals.